Solid-State Electronics 195 (2022) 108374

Contents lists available at ScienceDirect

Solid State Electronics

journal homepage: www.elsevier.com/locate/sse

Assessing the Effect of Scaling High-Aspect-Ratio ISFET with Physical Model Interface for Nano-Biosensing Application

Rakshita Dhar [a], Naveen Kumar [a], Cesar Pascual Garcia [b], Vihar Georgiev [a]

[a] Device Modelling Group, James Watt School of Engineering, University of Glasgow, UK
[b] Nano-Enabled Medicine and Cosmetics group, Materials Research and Technology Department, Luxembourg Institute of Science and Technology (LIST), Belvaux, Luxembourg

A B S T R A C T

In this paper, technology computer-aided design (TCAD) simulations of ion-sensitive field-effect transistors (ISFETs) are implemented using a physical model interface (PMI). Our simulations are based on a combination of analytical and numerical methods which are combined in a single simulation framework. ISFETs with different Si channel widths, such as 10nm, 40nm and 50nm have been simulated for this work. Our results reveal a correlation between the device dimensions and ISFET sensitivity (α). Also, the variations of H^+ ions, OH^- ions and surface potential (Ψ_0) with respect to distance from the electrolyte/oxide interface are analyzed

1. Introduction

Nano biosensors form an exciting field for the exploration of the combination of nano semiconductor devices and biomolecule/ion sensing in electrolyte solution [1,2]. One application of ion-sensitive field-effect transistor (ISFET) is biosensing which can be used for sensing biological charge variation in a chemical environment [3]. With further development of technology, novel ISFET devices have been fabricated for various applications [4]. However, there is still significant room to improve the ISFET sensitivity, reliability, and stability. The most time-efficient and cost-effective method to improve the ISFET technology is to perform simulations. In principle, the modeling can be divided into two categories: analytical and numerical. In this paper, we have used both approaches. An example for an analytical approach is so called site-binding model where the oxide/electrolyte interface forms an interface charged layer consisting of immobile ions. It calculates the surface charge density at the oxide/electrolyte interface corresponding to the potential developed due to H^+/OH^- ions [5]. An improved analytical approach is the Gouy-Chapman-Stern layer model, which takes into consideration the electrical double-layer [6].

2. Methodology

In this paper, our simulation approach is based on the implementation of the Gouy-Chapman-Stern layer model into an automated physical model interface (PMI) model of Synopsys Sentaurus TCAD which is similar to introducing trapped charges into oxide for every pH value [7]. We have designed a p-type metal oxide semiconductor (pMOS) structure to analyze the effect of oxide-electrolyte interactions. The introduction of the surface potential at the oxide-electrolyte interface is done using PMI instead of using trapped charges. PMI methodology allows us to decrease the simulation time and extreme values of pH e.g., 14 can be simulated. Also, in our simulation approach, we went one step further and introduced a Stern layer. At the moment, our simulation describes only the surface of the 2D-ISFET, but our methodology can further be extended to simulate a full-fledged 3D nano biosensor.

One of the parameters to measure ISFET device characteristics is sensitivity. The sensitivity (α) of the ISFET is defined based on the Gouy-Chapman-Stern layer model [8]. For $\alpha = 1$ means an ideal device, differential capacitance (C_{diff}) should be small and the intrinsic buffer capacity (β_{int}) should be high which depends on the number of surface binding sites and dissociation constants [2]. Another important parameter is the surface potential (Ψ_0). When an electrolyte interacts with the gate oxide, a potential is developed at the surface due to protonation and deprotonation of the surface reactive sites [9]. In the results sections, we have shown the details of how these parameters vary and what is the impact on the device performance.

The analytical models are implemented in MATLAB from where important device parameters are extacted. These prameters are used as an input data for the numerical simulations which are executed in Synopsys TCAD. The methodology described below is used to represent the surface charge at the oxide-electrolyte interface in TCAD simulations using PMI. In PMI, the capture and emission rates for electrons and holes - c_v^d, e_v^d, c_v^a, e_c^a are calculated by the analytical model equations as shown

E-mail addresses: r.dhar.1@research.gla.ac.uk (R. Dhar), Naveen.Kumar@glasgow.ac.uk (N. Kumar), cesar.pascual@list.lu (C. Pascual Garcia), Vihar.Georgiev@glasgow.ac.uk (V. Georgiev).

https://doi.org/10.1016/j.sse.2022.108374

Available online 4 May 2022

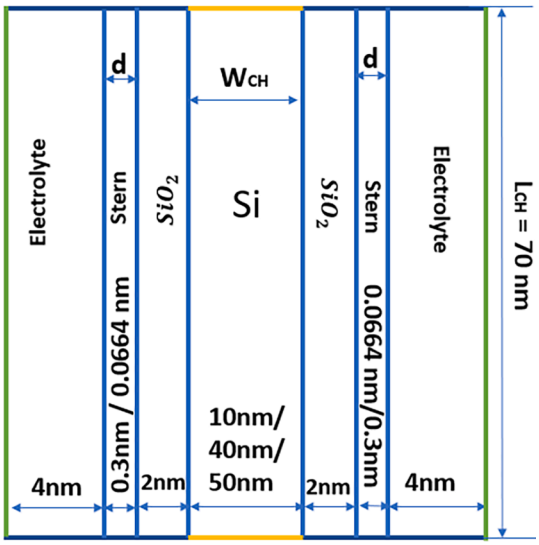

Fig. 1. 2D schematic diagram of the ISFET device simulated in TCAD environment with Stern layer thickness = 0.3 nm and 0.0664 nm channel and 70nm channel length while keeping the same dielectric constant for the Stern layer.

below;

$$c_v^d = cH_S^2 \tag{1}$$

$$e_v^d = K_a K_b + K_b cH_S \tag{2}$$

$$c_c^a = K_a K_b \tag{3}$$

$$e_c^a = K_b cH_S + cH_S^2 \tag{4}$$

where $cH_s = cH_B \exp(-q^*\Psi_0/kT)$ and $cH_B = [H_B^+] = 10^{-PH_B}$ M is the bulk hydrogen concentration. (5)

K_a and K_b are the surface dissociation parameters [2] used in simulations for SiO_2. The electrolyte is defined as an undoped semiconductor with relative permittivity $\varepsilon_{elec} = 80$ having a bandgap of 1.23 V since it's the electrolysis point of water. The salt ion molar concentration $c_0 = 0.1$ M. The electrolyte is considered to have equal number of positive and negative charges; hence, $N_c\ N_v = n_s\ p_s = c_0\ N_{av} = 0.1$ M x 10^{-3} cm^{-3} x 6.023×10^{23} $M^{-1} = 6.023 * 10^{19}$ cm^{-3} [10] where N_c is electron density of states, N_v is hole density of states and N_{av} is the Avogadro's constant. For stern layer [27], $\varepsilon_{stern} = 6$ as per the Gouy-Chapman-Stern theory to keep the stern capacitance with the range 0.2 F/m^2 to 0.8 F/m^2 [11].

To calculate the surface potential, we have developed the following analytical approach where we linked the surface charge density and the surface potential. The surface charge density σ_o in [2] is given by

$$\sigma_o = qN_S\left(\frac{cH_s^2 - K_a K_b}{K_a K_b + K_b cH_S + cH_S^2}\right) \tag{6}$$

Where N_S = total number of surface states (we are assuming 100% coverage), $cH_s = cH_B exp\frac{-q\Psi_0}{K_B T}$ is the surface hydrogen concentration, Ψ_0 is the surface potential (potential difference between the interface and the bulk) developed at the electrolyte-oxide interface (Ψ_0 is calculated by iterative method [12]), q is the electronic charge, K_B is Boltzmann constant and T is temperature. The distributed space charge density of double layer σ_{DL} as in [2] is given by

$$\sigma_{DL} = -(8kT\varepsilon_{elec}\varepsilon_0 n^0)^{\frac{1}{2}} sinh\left(\frac{zq\Psi_\xi}{2K_B T}\right) \tag{7}$$

Where n^0 is the concentration of ions in bulk solution and z represents the valency of the electrolyte (eg. Monovalent, z=1; Divalent, z=2;). By equating eq.6 with eq.7, an unknown variable zeta potential (Ψ_ξ) is obtained. Ψ_ξ when substituted in eq.8 gives the surface potential Ψ_0.

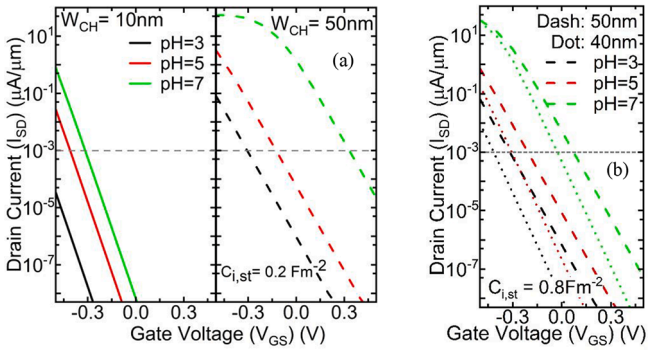

Fig. 2. I_{DS}-V_{GS} curve of the 2D ISFET device with a different channel widths (W_{CH}) (a) 10 nm and 50 nm and $C_{i,st} = 0.2$ F/m^2 (b) 40 nm and 50 nm and $C_{i,st} = 0.8$ F/m^2;Note: Graph scale is same for (a) and (b) for proper comparison with I_{SD} = 1nA/μm as the reference for graphs represented with dashed grey line

$$\Psi_0 = \Psi_\xi + \frac{(8kT\varepsilon_{elec}\varepsilon_0 n^0)^{1/2} sinh\frac{zq\Psi_\xi}{2K_B T}}{C_{i,st}} \tag{8}$$

where $C_{i,st}$ is intrinsic stern layer capacitance (0.2-0.8 F/m^2) [2,12]. The equation for surface potential variations (Ψ_{Var}) across the electrolyte has been derived and it is shown below.

$$\Psi_{Var} = 4V_T \times atanh\left(exp\left(\frac{-zd}{\lambda}\right) tanh\left(\frac{\Psi_\xi}{4V_T}\right)\right) \tag{9}$$

Where (thermal voltage) $V_T = \frac{K_B T}{q}$, zd is the distance away from oxide/electrolyte interface and λ is Debye length [13];

$$\lambda = \sqrt{\frac{\varepsilon_{elec} V_T}{2qn^0 N_{av}}} \tag{10}$$

3. Device Architecture and Material Properties

Fig. 1 shows the simulated ISFET structures. Si-channel width is varied with the same oxide thickness of 2nm and the electrolyte is 4nm wide. The stern layer thickness is varied to analyze the effect on the device characteristics. The stern layer width is 3 Å to keep the $C_{i,st} = 0.2$ F/m^2 and 0.664 Å to keep the $C_{i,st} = 0.8$ F/m^2. The yellow lines at the end of Si show the source/drain contact where V_{DS} (50mV) is applied. The vertical green lines at the sides of the electrolyte are gate contacts (reference electrode) where gate voltage (V_{GS}) is applied. The channel length (L_{CH}) of the device is taken to be 70 nm.

Fig. 2 shows the numerically calculated I_{DS}-V_{GS} curve for ISFETs with different channel widths. For the same W_{CH} (50 nm), the ISFET is more dominated by the surface potential as the I_{SD} is higher (saturated) even with lower stern capacitance as shown in Fig. 2(a) and Fig 2(b). As expected, when the pH of the electrolyte increases, the I_{DS}-V_{GS} curve shifts towards the higher gate voltages. This can be explained that since the channel has p-type doping, as the pH increases, the number of positive ions (H^+) in the electrolyte will decrease, hence the gate voltage required to turn-on the device moves towards more positive values. Also, Fig. 2 reveals that the sensitivity [ΔI_{DS} / (I_{DS} x ΔpH)] (normalized) of the device decreases as channel width increases which is consistent with the experimental results and previous works [12].

4. Results. *5. and Discussions*

From the simulation results, other than surface potential (Ψ_0) and zeta-potential (Ψ_ξ), we have obtained a sensitivity factor (α). Surface potential (Ψ_0) is defined as the potential developed at the interface between oxide and electrolyte. Zeta potential (Ψ_ξ) is the average potential developed at the plane of shear [2]. The sensitivity factor (α) is a

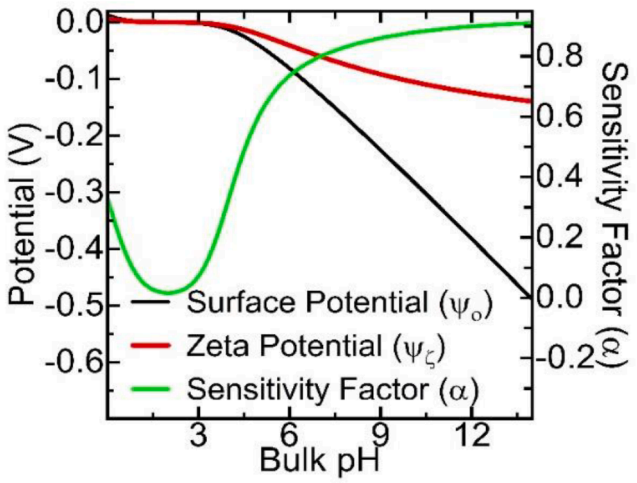

Fig. 3. Surface (black line), Zeta (red line) potential and sensitivity factor (green line) as a function of Bulk pH calculated from the analytical model consisting of Gouy-Chapman-Stern theory and Site-Binding theory.

dimensionless quantity ($0 < \alpha < 1$), that defines the response of the sensor based on the pH of the interacting electrolyte [12]. The equation used for α is

$$\alpha = \frac{1}{1 + \frac{2.303 K_B T C_{diff}}{q^2 \beta_{int}}} \tag{11}$$

where C_{diff} is the differential capacitance depending on electrolyte properties including stern layer and β_{int} is the dielectric intrinsic buffering capacitance which depends on the number of surface binding sites and affinity constants.

Fig. 3 shows the calculated changes of the surface potential (Ψ_0), zeta-potential (Ψ_ξ) and sensitivity factor (α) and a function of bulk pH value. For SiO_2, the point of zero-charge (pzc) is at pH = 2 where the surface potential and zeta potential are zero as shown in Fig. 3. With the increase in pH, the surface potential and zeta potential increase to higher negative values due to deprotonation of the silanol sites at the interface. The sensitivity factor depending on the change of surface potential with the pH variation acquires a non-linear behavior with opposite behavior to the potentials. A higher change in surface potential away from the pzc (pH = 2) with pH increases the value of α towards an ideal condition (α = 1).

Fig. 4(a) reveals the potential as a function of the distance away from the oxide/electrolyte interface within the electrolyte which is calculated based on equation (9). As the pH decreases, there are more negative charges on the surface, since the concentration of H^+ ions in solution decreases; hence, Ψ_ξ, Ψ_0 move to more negative values. Potential (– 've to +'ve) increases for higher pH and decreases for lower pH values after crossing the Debye length (1nm) due to repulsion from the charges present at the interface compared to the bulk that balances the potential to reach a minimum value (approx. 0V).

Using the information of the surface potential (Ψ_0), we have used Boltzmann distribution for the charge (H^+ or OH^-) concentration as a function of the distance of oxide/electrolyte interface:

$$p_{variation} = p_b \exp\left(\frac{-\Psi_{Var}}{V_T}\right) \tag{12}$$

$$n_{variation} = n_b \exp\left(\frac{\Psi_{Var}}{V_T}\right) \tag{13}$$

p_b and n_b is the concentration of H^+ and OH^- ions in bulk respectively. Fig. 4(b) presents the solutions to equation (12) considering various pH values. Based on the plot, it can be concluded that H^+ conc. increases away from the interface for pH < isoelectric point [point at which protonation and deprotonation remains in equilibrium resulting in zero charge] (i.e., 2 for SiO_2) and decreases for pH > isoelectric point due to the positive/negative potential at the interface at lower/higher pH values respectively. Also, the proton concentration (H^+) is inversely proportional to the OH^- concentration and the equation above describes such a relationship which again is using the information of the surface potential (Ψ_0) obtained as an initial value from equation (8). Fig. 4(c) reveals the results based on equation (13) where the OH^- concentration increases for higher pH value after crossing the Debye length away from the interface due to repulsion from the negative charges present at the interface and OH^- concentration gradient as compared to the bulk.

4. Conclusions

In this work, we have presented a method of implementing the Gouy-Chapman-Stern model using a physical-model-interface which allows us to implement the analytical equations into TCAD environment. Our simulations results reveal that the surface potential and sensitivity factor show a non-linear behavior at the oxide-electrolyte interface when pH changes. Also, we show that the variation of channel width is an important factor that can be used to tune the threshold voltage or current sensitivity of an ISFET. Moreover, we have shown our model can provide a 3D variation of the calculated potential in the electrolyte close to the sensor surface. This is the first step toward a 3D site-binding model which can take into account the effects of non-uniform charge distributions in molecules and represent the 3D molecular interactions (e.g., peptide-protein). Such hybrid analysis of an ISFET can pave way for designing novel chemosensors or biosensors.

Declaration of Competing Interest

The authors declare that they have no known competing financial

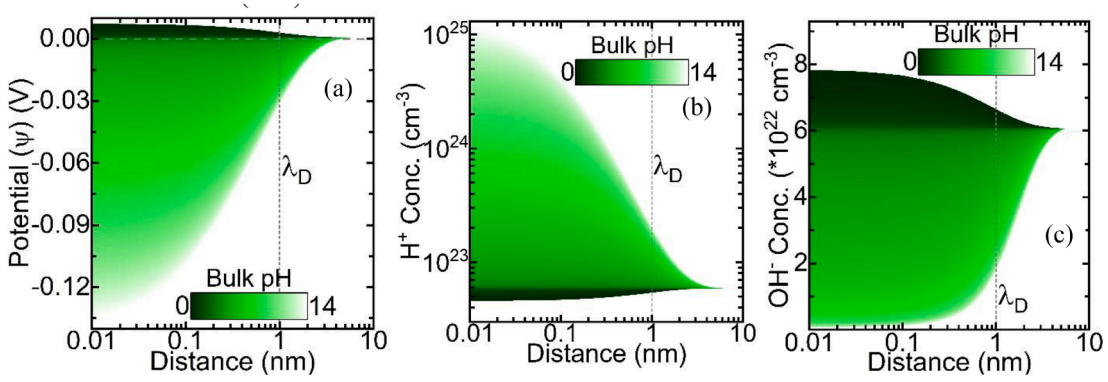

Fig. 4. (a) Potential (Ψ_{Var}) (b) Concentration of H^+ ions ($p_{variation}$) (c) Concentration of OH^- ions ($n_{variation}$) as a function of the distance away from the oxide/electrolyte interface calculated from the analytical model consisting of Gouy-Chapman-Stern theory and Site-Binding theory

interests or personal relationships that could have appeared to influence the work reported in this paper.

Acknowledgments

This project has received funding from the European Union's Horizon 2020 research and innovation program under grant agreement No 862539-Electromed-FET OPEN. Also, we would like to express gratitude to Pierpaolo Palestri and Mele Leandro Julian from University of Udine.

References

[1] Bergveld P. and A. Analytical and Biomedical Applications of Ion-Selective Field-Effect Transistors: Sibbald; 1988.
[2] van Hal REG, Eijkel JCT, Bergveld P. A general model to describe the electrostatic potential at electrolyte oxide interfaces. Advances in Colloid and Interface Science 1996;69(1):31–62.
[3] Bergveld P. Development of an Ion-Sensitive Solid-State Device for Neurophysiological Measurements. IEEE Transactions on Biomedical Engineering 1970;BME-17(1):70–1.
[4] Mohanty SS, et al. Hetero Channel Double Gate MOSFET for Label-free Biosensing Application. Silicon 2022:1–10.
[5] Yates DE, Levine S, Healy TW. Site-binding model of the electrical double layer at the oxide/water interface. Journal of the Chemical Society, Faraday Transactions 1: Physical Chemistry in Condensed Phases 1974;70:1807–18.
[6] Bard AJFLR, Electrochemical methods and applications.. New York. London: Wiley-Interscience; 2000.
[7] Dhar RPS, et al. TCAD Simulations of High-Aspect-Ratio Nano-biosensor for Label-Free Sensing Application. in *2021 Joint International EUROSOI Workshop and International Conference on Ultimate Integration on Silicon (EuroSOI-ULIS)*. 2021.
[8] Rollo S, Rani D, Leturcq R, Olthuis W, Pascual García C. High Aspect Ratio Fin-Ion Sensitive Field Effect Transistor: Compromises toward Better Electrochemical Biosensing. Nano Letters 2019;19(5):2879–87.
[9] Rollo S. A new design of an Electrochemical (bio)sensor. High Aspect Ratio Fin-FET. 2019.
[10] Bandiziol A, Palestri P, Pittino F, Esseni D, Selmi L. A TCAD-Based Methodology to Model the Site-Binding Charge at ISFET/Electrolyte Interfaces. IEEE Transactions on Electron Devices 2015;62(10):3379–86.
[11] Choi S, Mo H-S, Kim J, Kim S, Lee SM, Choi S-J, et al. Experimental Extraction of Stern-Layer Capacitance in Biosensor Detection Using Silicon Nanowire Field-Effect Transistors. Current Applied Physics 2020;20(6):828–33.
[12] Medina-Bailon C, Kumar N, Dhar RPS, Todorova I, Lenoble D, Georgiev VP, et al. Comprehensive Analytical Modelling of an Absolute pH Sensor. Sensors 2021;21(15):5190.
[13] Palazzo G, De Tullio D, Magliulo M, Mallardi A, Intranuovo F, Mulla MY, et al. Detection beyond Debye's length with an electrolyte-gated organic field-effect transistor. Advanced Materials 2015;27(5):911–6.